Letter

Quantum correlations, mixed states, and bistability at the onset of lasing

Francesco Papoff,[1,*] Mark Anthony Carroll,[1] Gian Luca Lippi,[2] Gian-Luca Oppo,[1] and Giampaolo D'Alessandro[3]
[1]*Department of Physics, University of Strathclyde, 107 Rottenrow, Glasgow G4 0NG, United Kingdom*
[2]*Université Côte d'Azur, Institut de Physique de Nice, UMR 7710 CNRS, 17, rue Julien Lauprêtre, 06200 Nice, France*
[3]*School of Mathematics, University of Southampton, Southampton SO17 1BJ, United Kingdom*

(Received 10 June 2024; accepted 17 December 2024; published 7 January 2025)

We derive a model for a single-mode laser that includes all two-particle quantum correlations between photons and electrons. In contrast to the predictions of semiclassical models, we find that lasing takes place in the presence of quantum bistability between a nonlasing and a nonclassical coherent state. The coherent state is characterized by a central frequency and a finite linewidth and emerges with finite amplitude from a saddle-node bifurcation together with an unstable coherent state. Hence coherent emission in nanolasers originates through a mixing of lasing and nonlasing states. In the limit of a macrolaser with a large number of emitters and nonresonant modes, the laser threshold approaches the prediction of the semiclassical theory, but with the important difference that lasing can be achieved only in the presence of finite-size perturbations.

DOI: 10.1103/PhysRevA.111.L011501

The development of nanolasers in recent years [1,2] has been driven by the demand for devices with a minimal footprint and thermal load for applications such as on-chip communications, sensing, and biological probes [3], with potential nonclassical applications enabled by photon number squeezing [4–6]. The size of these devices raises interesting fundamental questions about the identification of the lasing threshold [6–8] and the role of light-matter quantum correlations. These are expected to affect the dynamics and the statistics of light emission in nanolasers more strongly than in macroscopic lasers, where the large number of cavity modes and intracavity emitters ensure the validity of the semiclassical limit [9]. The search for performing models is of paramount importance at the nanoscale, where the challenging nature of the signals (low photon flux and large bandwidth) restricts the experimental information to the photon statistics. Reliable predictions become the only source for a meaningful comparison and interpretation of experimental results. For small numbers of emitters and electromagnetic field modes, laser quantum models become crucial under the requirement of overlapping their predictions with those of semiclassical theories when reaching the macroscopic scale.

Quantum models for nanolasers have been developed by using Heisenberg-Langevin equations [10], density matrix theory [11], nonequilibrium Green's functions [12], or by applying the cluster expansion [13], where the fast variables associated with coherent emission are neglected [4,14–16] and only the slowly varying quantum correlations are kept. These models have recently been extended within a semiclassical theory, by including the expectation values of the coherent field and the medium polarization, and by neglecting electron-electron and fast photon-electron quantum correlations [coherent-incoherent model (CIM)] [6,8]. The introduction of coherent variables has allowed us to identify a laser threshold, which can be experimentally detected by measuring the first-order correlation $g^{(1)}(\tau)$ [1], beyond which stimulated emission becomes continuous [17].

In this Letter we address two fundamental questions: to what extent do quantum correlations affect lasing, and whether models that include them can reduce to the semiclassical theory as the number of intracavity emitters grows. We consider all two-particle quantum correlations (photon-photon, photon-electron, and electron-electron) in a nanolaser model [4] containing quantum dots at a cryogenic temperature [two-particle model (TPM)]. The quantum dots have two localized levels where electrons and holes are injected from the wetting layer, and the light-matter coupling is weak. Coulomb [14,16] and phonon [18] scattering are considered through dephasing terms and the interaction Hamiltonian is simplified by keeping only terms that do not oscillate at the light frequency scale (rotating-wave approximation in the weak-coupling regime) [6,8]. The bosonic operators $b^\dagger$, b describe photon creation and annihilation processes, and the fermionic operators $c^\dagger$, c ($v^\dagger$, v) represent the upper (lower) energy level electron creation and annihilation. To understand the physical meaning of the theory, it is important to associate the operators with particles: $b^\dagger$, b are single-particle bosonic operators, while the single-particle fermionic operators [19] are composed of pairs of operators such as the electron number in the upper level, $c^\dagger c$, and the polarization, $c^\dagger v$.

The interaction between light and matter gives rise to an infinite hierarchy of differential equations for the expectation values of operators involving an increasing number of particles. The hierarchy can be truncated to a finite set by noting

*Contact author: f.papoff@strath.ac.uk

that the expectation value of any M-particle operator is the sum of an M-particle correlation—originated by processes involving all the M particles—and products of expectation values of operators with numbers of particles ranging from 1 to $(M-1)$ [19].

A detailed analysis of different approximation schemes has been performed in Ref. [20], where it was shown that some approximations can lead to nonphysical results such as negative populations of the excited state. Our model considers only two-particle correlations, which, in the weak-coupling regime, are expected to be larger than higher-order correlations [13] and we have verified that it produces physical results for both populations and photon numbers.

To implement this scheme we use the identity $\langle O_iO_jO_k\rangle = \langle O_iO_jO_k\rangle_{\mathcal{C}} + \langle O_iO_jO_k\rangle_{\mathcal{D}}$, where O_i, O_j, O_k are arbitrary one-particle operators, $\langle O_iO_jO_k\rangle_{\mathcal{C}}$ is the three-particle correlation, and $\langle O_iO_jO_k\rangle_{\mathcal{D}}$ the sum of products of single- and two-particle expectation values. We then truncate the equations at the two-particle level by setting $\langle O_iO_jO_k\rangle_{\mathcal{C}} = 0$. We apply this procedure to the exact (not-closed) equation

$$\frac{\mathrm{d}}{\mathrm{d}t}\begin{bmatrix}\langle O_i\rangle\\ \langle O_iO_j\rangle\end{bmatrix} = L\begin{bmatrix}\langle O_i\rangle\\ \langle O_iO_j\rangle\end{bmatrix} + \begin{bmatrix}\langle \mathcal{A}(O_i)\rangle\\ \langle \mathcal{A}(O_iO_j)\rangle\end{bmatrix} + \begin{bmatrix}0\\ R\langle O_iO_jO_k\rangle\end{bmatrix}, \tag{1}$$

where L is a square matrix, $\mathcal{A}$ accounts for the presence of nonresonant modes [Eqs. (S2) and (S3) in the Supplemental Material [21]], and R is a rectangular matrix that describes the coupling between two- and three-particle expectation values. The end result is an approximate (closed) system of equations obtained by replacing the last two terms in Eq. (1) by

$$\begin{bmatrix}\langle \mathcal{A}(O_i)\rangle\\ \langle \mathcal{A}(O_iO_j)\rangle\end{bmatrix} \longrightarrow \begin{bmatrix}\tilde{\mathcal{A}}(\langle O_i\rangle)\\ \tilde{\mathcal{A}}(\langle O_i\rangle\langle O_j\rangle)\end{bmatrix}, \tag{2a}$$

$$\begin{bmatrix}0\\ R\langle O_iO_jO_k\rangle\end{bmatrix} \longrightarrow \begin{bmatrix}0\\ R\langle O_iO_jO_k\rangle_{\mathcal{D}}\end{bmatrix}, \tag{2b}$$

where $\tilde{\mathcal{A}}$ are functions that give the radiative decay and pumping terms resulting from the adiabatic elimination of the correlations of the nonresonant modes with the polarization [see Eq. (12) in Ref. [16] and Eqs. (S10) and (S11) [21]]. While Eq. (1) is linear, the terms $\tilde{\mathcal{A}}(\langle O_i\rangle\langle O_j\rangle)$ and $R\langle O_iO_jO_k\rangle_{\mathcal{D}}$ are nonlinear. More generally, we can truncate the equations at any M number of particles by neglecting all correlations of $M+1$ particle operators [22,23], and thus approximate the eigenstates of a linear open quantum system of very large (possibly infinite) dimension with the stable steady states of a nonlinear system of much smaller dimension. For simplicity sake, we consider here a set of N identical single-electron quantum dots [24]. In this case, Eqs. (1) and (2) are equivalent to a set of 12 complex equations, the TPM equations with identical quantum dots [Eqs. (S12) [21]].

We determine the role of different two particle correlations by comparing the TPM and CIM predictions [8,17]. The CIM variables comprise three slow variables, electron number $\langle c^\dagger c\rangle$, photon-assisted polarization $\langle bc^\dagger v\rangle$, and photon number $\langle b^\dagger b\rangle$, and two complex fast variables oscillating at the laser frequency: coherent field amplitude $\langle b\rangle$ and polarization $\langle v^\dagger c\rangle$. The TPM has additional photon-electron and photon-photon fast variables including two photon-electron expectation values, namely $\langle bc^\dagger c\rangle$, and $\langle bv^\dagger c\rangle$, and one fast photon-photon expectation value $\langle bb\rangle$. Additionally, it has electron-electron expectation values comprising two slow variables, $\langle c^\dagger v^\dagger cv\rangle$, $\langle c^\dagger c^\dagger cc\rangle$, and two fast variables, $\langle v^\dagger c^\dagger cc\rangle$, $\langle v^\dagger v^\dagger cc\rangle$. We model phonon scattering by adding a dephasing term to electron-electron expectation values, $\mu\gamma$, with $\mu \geqslant 0$, following Ref. [18], where it was shown that this dephasing reproduces the key effects of a microscopic theory of phonon scattering. The other control parameters are common to all models: the light-matter coupling g; the decay rates of the upper-level population due to nonradiative processes, γ_{nr}, and nonlasing modes, γ_{nl}; the dephasing rate of the polarization, γ; the pump rate per emitter, r; and the number of quantum dots N inside the laser. All the parameter values have been chosen based on experimental considerations (see Sec. SVII [21]). For both CIM and TPM we characterize the lasing solution using its coherence time, which can be experimentally measured through the visibility of interference fringes [1]. The richer nonlinear structure of the TPM with respect to the CIM equations is expected to lead to multistability, which, as shown in similar situations [25–27], corresponds to mixed states in the open quantum system.

In Fig. 1 we show the absolute value of the amplitude of the coherent field, $|\langle b\rangle|$, versus the ratio of the pump rate per emitter and the nonradiative decay rate, r/γ_{nr}, for nanolasers with $N = 25$ [Fig. 1(a)] and $N = 500$ [Fig. 1(b)], computed by integrating Eqs. (S14) [21]. The vertical bars, of length equal to the generalized standard deviation $\sqrt{|\langle bb\rangle - \langle b\rangle^2|}$, illustrate both the variation of the values of $|\langle b\rangle|$ and that this state is not a Glauber coherent state—the analog of a coherent classical field with $\langle bb\rangle - \langle b\rangle^2 = 0$—but a nonclassical Gaussian state [28]. The key result is that for the TPM the coherent field has always a finite threshold amplitude, while this is zero in the semiclassical CIM (solid blue line).

Electron-electron correlations increase both the thresholds and the generalized standard deviation even for a large number of QDs. These effects, however, are severely reduced by the presence of a small amount of phonon scattering, e.g., the $\mu = 0.05$ curves in Fig. 1. This sensitivity is in agreement with the results of Refs. [18,29]. In the presence of phonon scattering, the amplitude of the coherent field approaches that of the semiclassical theory as the number of emitters increases. A similar dependence on quantum correlations of the dynamics of large numbers of particles has been recently found also in spin systems [30].

Furthermore, contrary to what happens in the semiclassical theory, there are two lasing solutions, one stable and one unstable, that appear at the lasing threshold (Fig. 2). The real part of only one eigenvalue of the Jacobian matrix changes sign at this point, which can therefore be classified as a saddle-node bifurcation of limit cycles. The bifurcation appears when the correlation between the population of the upper level and the field—a nonclassical correlation emerging from the interaction between field and quantum dots—is introduced, even if all other correlations are neglected. We have verified numerically in the physically relevant pump value ranges used in this Letter, that there are two observable stable states, one with coherent emission and the other without, and an unstable state. Physically, the unstable state is a state with

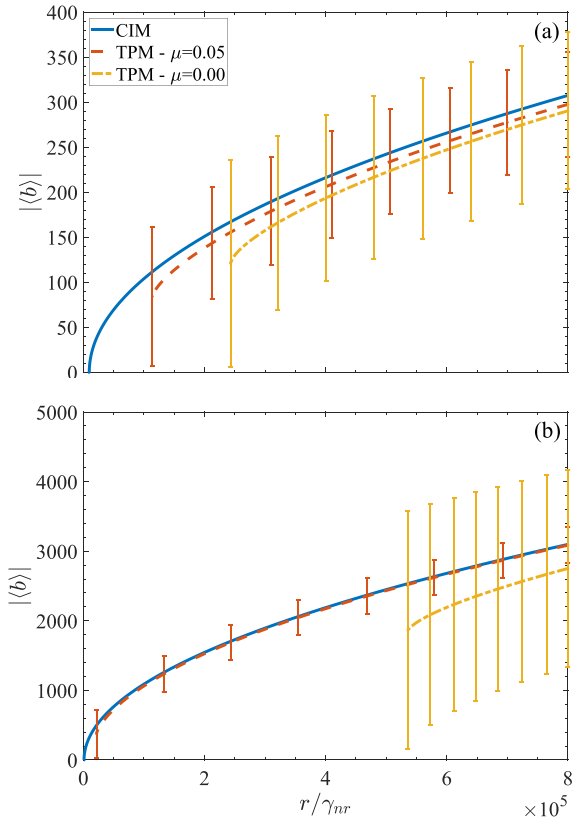

FIG. 1. Lasing solutions for the CIM (solid blue line) and the TPM (dashed lines, yellow for $\mu = 0$, red for $\mu = 0.05$) with (a) $N = 25$ and (b) $N = 500$. The thin vertical lines measure the generalized standard deviation $\sqrt{|\langle bb\rangle - \langle b\rangle^2|}$. Time, decay rates, and coupling parameters are scaled with $\gamma_{\rm nr} = 10^{-9}$ s^{-1}. Other parameter values (common to all figures) are $g = 70$, $\Delta\nu = 0$, $\gamma = 10^4$, $\gamma_c = 10$, and $\gamma_{\rm nl} = 0$ (equivalent to $\beta = 1$).

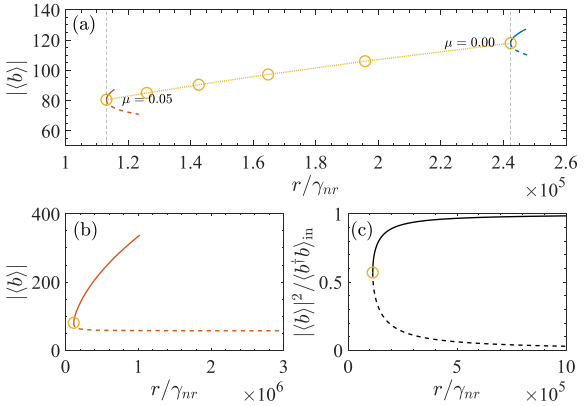

FIG. 2. (a) Bifurcation diagram of the TPM lasing solution (stable, solid, unstable, dashed) for $N = 25$ as a function of the pump for $\mu = 0.00$ (blue lines) and $\mu = 0.05$ (red lines). The bifurcation points where the stable and unstable solutions meet are the lasing thresholds. They are indicated by open circles for equally spaced values of μ in the range [0,0.05]. The incoherent solution $|\langle b\rangle| = 0$ (not shown) is stable. The dotted line is only a guide for the eye. The vertical dashed lines show the analytical values of the threshold provided by Eq. (3). (b) Extension of the bifurcation diagram in (a) for the case $\mu = 0.05$ showing that the unstable lasing solution approaches the incoherent solution, but remains bounded away from it. (c) Plot of the ratio $|\langle b\rangle|^2/\langle b^\dagger b\rangle_{\rm in}$ for the stable (solid) and unstable (dashed) lasing solutions, where $\langle b^\dagger b\rangle_{\rm in}$ is the photon number of the incoherent solution ($\langle b\rangle = 0$) at the same pump value.

coherent emission and extremely short lifetime that acts as a separatrix between the incoherent and the stable laser solution in the one-dimensional center manifold of the lasing bifurcation where the slow dynamics takes place. Even though the unstable coherent solution seems to tend to a finite nonzero value [see Fig. 2(b)], the ratio of the amplitude squared of its coherent field with respect to the incoherent solution photon number tends to zero [see Fig. 2(c)]. This indicates that the incoherent solution will be destabilized by perturbations with smaller and smaller relative amplitudes as the pump parameter increases.

An accurate analytical estimate of the laser threshold (vertical dashed lines in Fig. 2) is found from the analytical solution of the incoherent state,

$$r_{\rm th} = \left(\Gamma_n + \frac{\Gamma_g}{K}\right)\frac{\langle c^\dagger c\rangle_{\rm th}}{1 - \langle c^\dagger c\rangle_{\rm th}}, \tag{3}$$

where $\langle c^\dagger c\rangle_{\rm th}$ is the CIM threshold value, Eq. (S.29) [21], $\Gamma_n = \gamma_{\rm nr} + \gamma_{\rm nl}$, $\Gamma_g = 2g^2(\gamma + \gamma_c)/[(\gamma + \gamma_c)^2 + \Delta\nu^2]$, and $K = 1 - \Gamma_g(2\langle c^\dagger c\rangle_{\rm th} - 1)\{N/2\gamma_c + (N-1)/[2\gamma(1+\mu)]\}$.

For completeness, we note there are other ways to define the threshold [31], which appear to identify different points in the transition from incoherent to coherent emission in nanolasers and behave differently from very large values of g. Equations (3) and (S29) [21] identify the appearance of a stable coherent solution with constant amplitude; based on Ref. [32] we expect that below this threshold, transients of coherent emission are possible and can lead to a gradual increase of time-averaged measures of the coherence as the pump approaches the threshold value. Moreover, the nonlasing solution continues to be linearly stable above the lasing threshold. It should be noted that this bistability does not appear in the semiclassical limit, where, in a framework where quantum correlations vanish, bistability is associated with a first-order phase transition. Here, however, bistability is a consequence of the inclusion of two-particle quantum correlations and indicates the presence of a mixing of lasing and nonlasing states in nanolasers far from the semiclassical limit. In Fig. 2 we also plot the effect of phonon scattering on the lasing threshold. For all values of μ plotted there are stable and unstable lasing solutions at the threshold. This implies that the bistability is present also when the laser threshold and the $|\langle b\rangle|$ curve approach the semiclassical theory, showing that lasing can be started only by finite amplitude perturbations.

To illustrate further the difference between the CIM and TPM lasing and nonlasing solutions and the impact these have on nano- and macrolasers, we plot their first-order coherence time, τ_c, defined in Eq. (S17) [21], for a nano- and a macrolaser, Figs. 3(a) and 3(b), respectively. For all nonlasing solutions $g^{(1)}(\tau)$ is calculated from a system of linear differential equations, derived from the CIM and TPM equations using the quantum regression [33] theory. In this approach each CIM or TPM equation for a variable $\langle O(t)\rangle$ leads to a linear

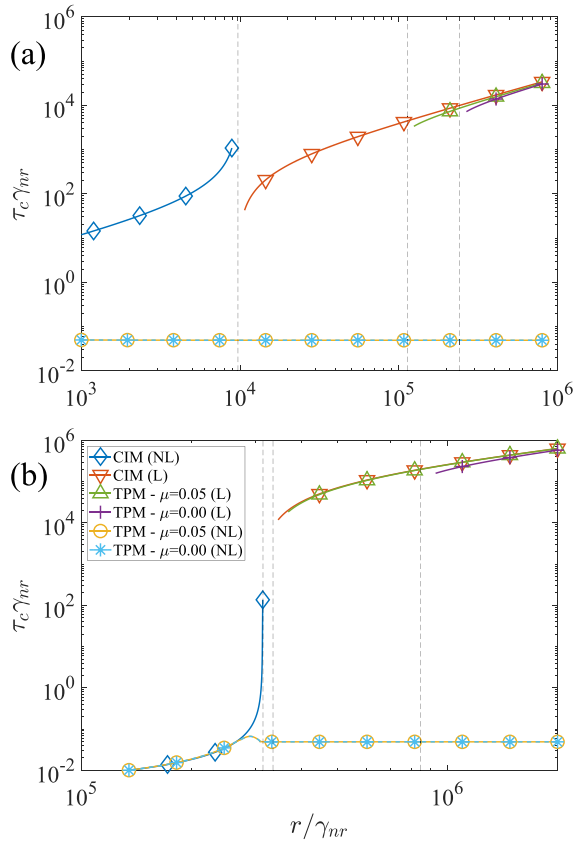

FIG. 3. Decay time of the first-order correlation function, τ_c, for lasing (L) and nonlasing (NL) CIM and TPM solutions for (a) a nanolaser and (b) a macrolaser. The vertical dashed lines show from left to right the analytical values of the threshold, Eq. (3), for the CIM, TPM $\mu = 0.05$, and TPM $\mu = 0.00$ lasing solutions. The correlation time of the CIM (NL) solution diverges at threshold. The CIM (NL) and TPM (NL) curves were computed using Eqs. (S27) and (S24), respectively [21]. The TPM (L) curves were computed using the Schawlow-Townes theory, Eq. (S25) [21], and plotted only for pump values at least 10% above threshold. The parameters are $\beta = 1$ and $N = 25$ for the nanolaser in (a), and $\beta = 3.4 \times 10^{-6}$ and $N = 500$ for the macrolaser in (b). All other parameters are as in Fig. 1.

differential equation for the mixed time expectation value $\langle b^\dagger(t)O(t+\tau)\rangle$, where τ is the delay time [17,34]. For the CIM and TPM nonlasing solutions this approach leads to a 2×2 and a 5×5 system, respectively [Eqs. (S27) and (S24) [21]]. Unfortunately, this approach is not suitable for the lasing solutions. These are phase-rotation invariant and, hence, their decoherence is dictated by slow fluctuations of the phase [35,36]. Mathematically, the invariance implies that the linear equations have a zero eigenvalue and it is not straightforward to use this theory to study their (slow) dynamics in the corresponding manifold. Therefore, we follow the approach of Ref. [37], where it is shown that, for systems such as those considered here in which the polarization decays much faster than the other variables [see Eqs. (24) and (30) in Ref. [37]], τ_c can be estimated by the Schawlow-Townes formula [Eq. (S25) [21]].

The coherence time of the CIM nonlasing solution, CIM (NL), diverges at the threshold. This is due to the nature of the CIM lasing transition: The nonlasing solution changes its stability and the stable lasing solution appears with zero amplitude. As the transition point is approached the fluctuations become slower and the coherence time diverges. This is not the case of the TPM nonlasing solution, TPM (NL), which remains always stable and with a finite and small coherence time. The lasing solutions of either model, CIM (L) and TPM (L), have similar behaviors: Their τ_c are much larger than the nonlasing solutions and increase with the pump.

Because of the bistability between TPM (L) and TPM (NL) solutions, even above threshold a nanolaser will be in a mixture of these two states and, therefore, its coherence will be a combination of theirs. In particular, the experimentally observed smooth increase in correlation as the bifurcation is approached [1] can be explained in terms of mixed lasing and nonlasing states with the weight of the lasing state component increasing with the pump.

An experimental verification of the bifurcation diagram in Fig. 2 can be obtained from the distributions of the experimental measures of light coherence at different pump values. From an experimental point of view, the expected temporal scales over which noise tips a nanolaser away from the stable incoherent state are nowadays accessible. As an estimate, we can assume the cavity buildup time as the needed (minimal) timescale. Since the current photon statistical apparatus has a temporal resolution better than 10 ps, it is possible to construct lasers where the statistics can be experimentally collected. The scheme would consist in collecting emission levels [possibly with spectral information through interferometric measurements of $g^{(1)}(\tau)$] by repeatedly modulating the laser across the threshold and accumulating a probability density function (PDF) of the collected photon number (and/or coherence level). The measurement could be performed either at a fixed time—detecting the population of the two states (incoherent and coherent emission) which present well-separated peaks in coherence times—or in collecting the statistics of the time delay for threshold crossing. The expected results would have a form similar to that found in the transient bimodality in optical bistability as predicted in Ref. [38] and observed in Ref. [39].

We conclude the analysis of the TPM (L) solutions with a study of their frequency. The steady state single-mode lasing frequency Ω, derived analytically in Sec. SVI [21], is

$$\Omega = \nu + \gamma_c \frac{\mathrm{Im}(\langle v^\dagger c\rangle^* \langle b\rangle)}{\mathrm{Re}(\langle v^\dagger c\rangle^* \langle b\rangle)}. \tag{4}$$

In the case of the CIM this formula simplifies to $\Omega^{(\mathrm{CIM})} = \nu + \gamma_c \Delta\nu/(\gamma_c + \gamma)$ [8], which appears to be also an excellent approximation of the TPM (L) frequency, as shown in Fig. 4.

In conclusion, we have observed that in the TPM, i.e., a model that includes two-particle quantum correlations, lasing appears through a saddle-node bifurcation of limit cycles for both nano- and macrolasers. Furthermore, incoherent and coherent states are bistable, and the lasing solutions have a finite linewidth. For nanolasers with a small number of QDs, quantum effects result in a significant departure from semiclassical

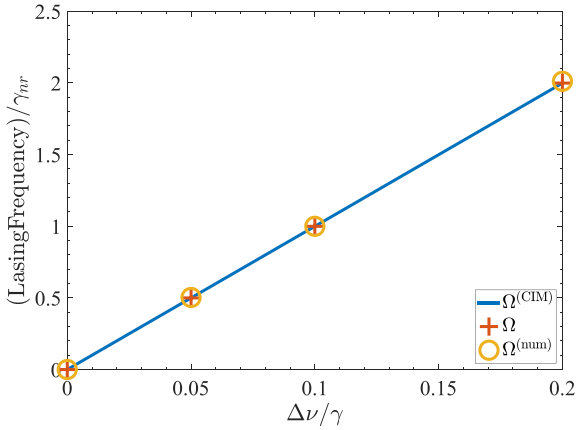

FIG. 4. Frequency vs detuning $\Delta\nu$ for the CIM and TPM (with $\mu = \{0.00, 0.05\}$) lasing solutions. The solid line is the analytical CIM frequency $\Omega^{(CIM)}$. The + markers are the CIM and TPM lasing frequencies computed using Eq. (4) averaged over $100/\gamma_{nr}$ s. The circle markers are the frequency computed by taking the dominant peak in the power spectrum of the numerical solution of the coherent field $\langle b\rangle$ averaged over the same time interval. The differences between the CIM and the two TPM simulations are not visible on the scale of the graph. All parameters are as in Fig. 1 except that $r/\gamma_{nr} = 8 \times 10^5$.

theories; the same effects are present also in macrolasers, but are much harder to observe. From the perspective of applications, this affects key properties such as the signal-to-noise ratio as well as the buildup or collapse of coherence that are crucial in all applications where coherence is essential, such as spectroscopy, and in those involving ramping up or down of the laser parameters, such as data processing and storing. The nonclassical nature of the coherent states and the quantum correlations described here can have practical applications in continuous-variable quantum technologies which rely on Gaussian states. Nonclassical Gaussian states, present both in the CIM [6] and in the TPM, can lead to entanglement, as recently proven with two-mode Gaussian states [40]. The advantages of nanolasers is that they can be integrated into photonic chips leading to portable quantum optical devices [41]. Furthermore, the theory provides measurable quantities such as laser frequency and linewidth that allow one to identify emission processes and laser threshold. We remark that the predicted bistability is consistent with the experimental observation of spontaneous photon burst emission at the threshold of microlasers [42,43] for which no first-principles theory has been previously identified. Finally, preliminary numerical simulations show that the condition of identical QDs can be relaxed without changing the scenario described in this Letter even without fermionic correlations, which indicates that the effect should be observable even at higher temperatures. The bifurcation scheme emerging from this Letter also suggests different topologies in which to study delay-controlled bifurcations and their shifts. This topic, outlined for lasers in Ref. [44], is of great interest and finds applications in a broad variety of fields (see, e.g., Refs. [45,46]) and is very actively pursued for its potential applications. Lasers present considerable advantages over other systems—irrespective of their nature—given their stability and reproducibility, in addition to the easy and rapid data collection. The features of this bifurcation offer an alternative scenario for the acquisition of information on different schemes. Finally, we can envisage forms of control of the bifurcation switch towards lasing, for instance through the injection of light pulses into the laser, to ensure a rapid transition through threshold for low desired emission levels.

We thank Peter Kirton and John Jeffers for many illuminating discussions

[1] J.-S. Tempel, I. Akimov, M. Aßmann, C. Schneider, S. Höfling, C. Kistner, S. Reitzenstein, L. Worschech, A. Forchel, and M. Bayer, Extrapolation of the intensity autocorrelation function of a quantum-dot micropillar laser into the thermal emission regime, J. Opt. Soc. Am. B **28**, 1404 (2011).

[2] A. Koulas-Simos, J. Buchgeister, M. L. Drechsler, T. Zhang, L. K, G. Sinatkas, J. Xu, F. Lohof, Q. Kan, R. K. Zhang, F. Jahnke, C. Gies, W. W. Chow, C.-Z. Ning, and S. Reitzenstein, Quantum fluctuations and lineshape anomaly in a high-β silver-coated InP-based metallic nanolaser, Laser Photonics Rev. **16**, 2200086 (2022).

[3] R.-M. Ma and R. F. Oulton, Applications of nanolasers, Nat. Nanotechnol. **14**, 12 (2019).

[4] S. Kreinberg, W. W. Chow, J. Wolters, C. Schneider, C. Gies, F. Jahnke, S. Höfling, M. Kamp, and S. Reitzenstein, Emission from quantum-dot high-β microcavities: Transition from spontaneous emission to lasing and the effects of superradiant emitter coupling, Light: Sci. Appl. **6**, e17030 (2017).

[5] J. Mork and K. Yvind, Squeezing of intensity noise in nanolasers and nanoLEDs with extreme dielectric confinement, Optica **7**, 1641 (2020).

[6] M. Carroll, G. D'Alessandro, G. Lippi, G.-L. Oppo, and F. Papoff, Photon-number squeezing in nano- and microlasers, Appl. Phys. Lett. **119**, 101102 (2021).

[7] C.-Z. Ning, What is laser threshold? IEEE J. Sel. Top. Quantum Electron. **19**, 1503604 (2013).

[8] M. A. Carroll, G. D'Alessandro, G. L. Lippi, G.-L. Oppo, and F. Papoff, Thermal, quantum antibunching and lasing thresholds from single emitters to macroscopic devices, Phys. Rev. Lett. **126**, 063902 (2021).

[9] N. B. Abraham and L. M. Narducci, *Laser Physics and Laser Instabilities* (World Scientific, Singapore, 1988).

[10] I. E. Protsenko and A. V. Uskov, Perturbation approach in Heisenberg equations for lasers, Phys. Rev. A **105**, 053713 (2022).

[11] A. M. Yacomotti, Z. Denis, A. Biella, and C. Ciuti, Quantum density matrix theory for a laser without adiabatic elimination of the population inversion: Transition to lasing in the class-B limit, Laser Photonics Rev. **17**, 2200377 (2023).

[12] A. A. Vyshnevyy, Gain-dependent Purcell enhancement, breakdown of Einstein's relations, and superradiance in nanolasers, Phys. Rev. B **105**, 085116 (2022).

[13] J. Fricke, Transport equations including many-particle correlations for an arbitrary quantum system: A general formalism, Ann. Phys. **252**, 479 (1996).

[14] W. Chow and F. Jahnke, On the physics of semiconductor quantum dots for applications in lasers and quantum optics, Prog. Quantum. Electron. **37**, 109 (2013).

[15] W. Chow, F. Jahnke, and C. Gies, Emission properties of nanolasers during the transition to lasing, Light: Sci. Appl. **3**, e201 (2014).

[16] C. Gies, J. Wiersig, M. Lorke, and F. Jahnke, Semiconductor model for quantum-dot-based microcavity lasers, Phys. Rev. A **75**, 013803 (2007).

[17] M. A. Carroll, G. D'Alessandro, G. L. Lippi, G.-L. Oppo, and F. Papoff, Coherence buildup and laser thresholds from nanolasers to macroscopic lasers, Phys. Rev. A **107**, 063710 (2023).

[18] N. Baer, C. Gies, J. Wiersig, and F. Jahnke, Luminescence of a semiconductor quantum dot system, Eur. Phys. J. B **50**, 411 (2006).

[19] M. Kira and S. W. Koch, *Semiconductor Quantum Optics* (Cambridge University Press, Cambridge, UK, 2011).

[20] M. Sánchez-Barquilla, R. E. F. Silva, and J. Feist, The potential and global outlook of integrated photonics for quantum technologies, J. Chem. Phys. **152**, 034108 (2020).

[21] See Supplemental Material at http://link.aps.org/supplemental/10.1103/PhysRevA.111.L011501 for all the model equations used in this Letter, the details of the calculations of the first-order correlation, the laser threshold and frequency, and typical parameter values.

[22] H. A. Leymann, A. Foerster, and J. Wiersig, Expectation value based cluster expansion, Phys. Status Solidi C **10**, 1242 (2013).

[23] H. A. M. Leymann, A. Foerster, and J. Wiersig, Expectation value based equation-of-motion approach for open quantum systems: A general formalism, Phys. Rev. B **89**, 085308 (2014).

[24] C. B. Simmons, M. Thalakulam, N. Shaji, L. J. Klein, H. Qin, R. H. Blick, D. E. Savage, M. G. Lagally, S. N. Coppersmith, and M. A. Eriksson, Single-electron quantum dot in Si/SiGe with integrated charge sensing, Appl. Phys. Lett. **91**, 213103 (2007).

[25] M. V. Ivanchenko, E. A. Kozinov, V. D. Volokitin, A. V. Liniov, I. B. Meyerov, and S. V. Denisov, Classical bifurcation diagrams by quantum means, Ann. Phys. **529**, 1600402 (2017).

[26] N. Bartolo, F. Minganti, W. Casteels, and C. Ciuti, Exact steady state of a Kerr resonator with one- and two-photon driving and dissipation: Controllable Wigner-function multimodality and dissipative phase transitions, Phys. Rev. A **94**, 033841 (2016).

[27] W. Casteels, R. Fazio, and C. Ciuti, Critical dynamical properties of a first-order dissipative phase transition, Phys. Rev. A **95**, 012128 (2017).

[28] S. Olivares, Quantum optics in the phase space - A tutorial on Gaussian states, Eur. Phys. J. Spec. Top. **203**, 3 (2012).

[29] M. A. Carroll, G. D'Alessandro, G. L. Lippi, G.-L. Oppo, and F. Papoff, Carroll *et al.* reply: Thermal, quantum antibunching and lasing thresholds from single emitters to macroscopic devices, Phys. Rev. Lett. **128**, 029402 (2022).

[30] P. Fowler-Wright, K. B. Arnardóttir, P. Kirton, B. W. Lovett, and J. Keeling, Determining the validity of cumulant expansions for central spin models, Phys. Rev. Res. **5**, 033148 (2023).

[31] M. Saldutti, Y. Yu, and J. Mórk, The onset of lasing in semiconductor nanolasers, Laser Photonics Rev. **18**, 2300840 (2024).

[32] G. Habib, Predicting saddle-node bifurcations using transient dynamics: A model-free approach, Nonlinear Dynamics **111**, 20579 (2023).

[33] H. Carmichael, *Statistical Methods in Quantum Optics I* (Springer, Heidelberg, 2002).

[34] S. Ates, C. Gies, S. M. Ulrich, J. Wiersig, S. Reitzenstein, A. Löffler, A. Forchel, F. Jahnke, and P. Michler, Influence of the spontaneous optical emission factor β on the first-order coherence of a semiconductor microcavity laser, Phys. Rev. B **78**, 155319 (2008).

[35] C. Henry, Phase noise in semiconductor lasers, J. Lightwave Technol. **4**, 298 (1986).

[36] I. E. Protsenko, A. V. Uskov, E. C. André, J. Mørk, and M. Wubs, Quantum Langevin approach for superradiant nanolasers, New J. Phys. **23**, 063010 (2021).

[37] A. S. Chirkin and A. V. Chipouline, Generalized expression for the natural width of the radiation spectrum of quantum oscillators, JETP Lett. **93**, 114 (2011).

[38] G. Broggi and L. A. Lugiato, Transient noise-induced optical bistability, Phys. Rev. A **29**, 2949 (1984).

[39] W. Lange, F. Mitschke, R. Deserno, and J. Mlynek, Study of fluctuations in transient optical bistability, Phys. Rev. A **32**, 1271 (1985).

[40] B. Li, A. Das, S. Tserkis, P. Narang, P. K. Lam, and S. M. Assad, Quantum density matrix theory for a laser without adiabatic elimination of the population inversion: Transition to lasing in the class-B limit, Sci. Rep. **13**, 11722 (2023).

[41] E. Pelucchi, G. Fagas, I. Aharonovich, D. Englund, E. Figueroa, Q. Gong, H. Hannes, J. Liu, C.-Y. Lu, N. Matsuda, J.-W. Pan, F. Schreck, F. Sciarrino, C. Silberhorn, J. Wang, and K. D. Jöns, The potential and global outlook of integrated photonics for quantum technologies, Nat. Rev. Phys. **4**, 194 (2022).

[42] T. Wang, G. Puccioni, and G. Lippi, Dynamical buildup of lasing in mesoscale devices, Sci. Rep. **5**, 15858 (2015).

[43] T. Wang, G. Wang, G. P. Puccioni, and G. L. Lippi, Exploration of VCSEL ultra-low biasing scheme for pulse generation, J. Opt. Soc. Am. B **36**, 799 (2019).

[44] J. R. Tredicce, G. L. Lippi, P. Mandel, B. Charasse, A. Chevalier, and B. Picqué, Critical slowing down at a bifurcation, Am. J. Phys. **72**, 799 (2004).

[45] M. Scheffer, S. R. Carpenter, T. M. Lenton, J. Bascompte, W. Brock, V. Dakos, J. van de Koppel, I. A. van de Leemput, S. A. Levin, E. H. van Nes, M. Pascual, and J. Vandermeer, Anticipating critical transitions, Science **338**, 344 (2012).

[46] G. Zeng, J. Gao, L. Shekhtman, S. Guo, W. Lv, J. Wu, H. Liu, O. Levy, D. Li, Z. Gao, H. E. Stanley, and S. Havlin, Multiple metastable network states in urban traffic, Proc. Natl. Acad. Sci. USA **117**, 17528 (2020).